Journal of ELECTRONIC MATERIALS, Vol. 49, No. 9, 2020
https://doi.org/10.1007/s11664-020-08313-5
© 2020 The Minerals, Metals & Materials Society

TOPICAL COLLECTION: 18TH CONFERENCE ON DEFECTS (DRIP XVIII)

Three-Dimensional Observation of Internal Defects in a β-Ga_2O_3 (001) Wafer Using the FIB–SEM Serial Sectioning Method

KENICHI OGAWA,[1,3] NAOYA OGAWA,[1] RYO KOSAKA,[1] TOSHIYUKI ISSHIKI,[1] YONGZHAO YAO,[2] and YUKARI ISHIKAWA[2]

1.—Kyoto Institute of Technology, Matsugasaki, Sakyo-Ku, Kyoto 606-8585, Japan. 2.—Japan Fine Ceramics Center, 2-4-1 Mutsuno, Atsuta-ku, Nagoya 456-8587, Japan. 3.—e-mail: ogawa1kbd6@gmail.com

We reported our observation results on the etch pit shapes on β-Ga_2O_3 (001) wafers using a scanning electron microscope (SEM) and an atomic force microscope (AFM) in a previous study. However, it was difficult to detect the internal crystal defects that exist under the etch pits. In this study, to gain a detailed understanding of the internal crystal defects under the etch pits in detail, we observed the etch pits on the (001) surface three-dimensionally using a focused ion beam–SEM. The etch pits investigated were "Cicada I" and "Cicada II," which had the characteristic shapes observed in previous SEM and AFM analysis. Using this method, we revealed the existence of plate-like defects along the (100) plane under the etch pits. The proposed method is useful for understanding internal defects the etch pits which cannot be clarified by observing the surface using SEM and AFM analysis. Furthermore, from the changes in the SEM image contrast, Cicada I and Cicada II were deduced to be internal planar defects, i.e., plate-like voids and stacking faults, respectively.

Key words: Gallium oxide (Ga_2O_3), etch pit, crystal defects, focused ion beam–scanning electron microscope (FIB–SEM)

INTRODUCTION

Gallium oxide (Ga_2O_3) is a transparent oxide semiconductor with a wider electron bandgap than silicon carbide (SiC, 3.3 eV) and gallium nitride (GaN, 3.4 eV). Therefore, Ga_2O_3 is considered a key material in next-generation high-power electronics. Ga_2O_3 has five crystal polymorphisms: α, β, γ, δ, and ε, of which β-Ga_2O_3 is the most stable. The unit cell of a β-Ga_2O_3 belongs to the monoclinic system, where $a = 1.223$ nm, $b = 0.304$ nm, $c = 0.580$ nm, and $\beta = 103.83°$.[1,2] β-Ga_2O_3 can be grown from melt sources. Therefore, larger crystals can be produced more economically than SiC and GaN. The use of the edge-defined film-fed growth method that is already being employed in the mass production of sapphire wafers is also beneficial.[3,4]

The control of crystal defects is an important issue in substrate development because it affects device performance. Therefore, various studies on defects in β-Ga_2O_3 substrates have been reported.[2,5–10] Nakai et al.[5] reported two types of defects in β-Ga_2O_3 using chemical etching and transmission electron microscopy (TEM), i.e., screw dislocations and nanopipes (010). Ueda et al.[6] reported the existence of an array of edge dislocations aligned in the [010] direction and twin lamellae using chemical etching, TEM, and scanning electron microscopy (SEM). Yamaguchi et al.[9,10] reported the presence of stacking faults (SFs) on a (−201) plane using x-ray topography. These studies

(Received January 21, 2020; accepted July 2, 2020; published online July 18, 2020)

used substrates that were grown by pulling in the [010] direction with (−2,01) as the principal surface. However, there have been few reports on recently commercialized substrates having the (001) plane as the principal surface. In this background, we have reported our observation results on the etch pit shapes on a β-Ga_2O_3 (001) wafer using SEM and atomic force microscopy (AFM).[11] This study was successful in classifying six differently shaped etch pits. As shown in Fig. 1, they were named "Cicada I," "Cicada II," "Cannon ball," "Trapezoid," "Bar," and "Shell." The etch pits of Cicada I and Cicada II had a characteristic shape with a "plate-like pit" that was inclined at an angle of approximately 76° with respect to the (001) plane. Figure 2 shows the cross-sectional depth profiles along the [−100] direction of the Cicada I- and Cicada II-type etch pits. The main difference between these two types of etch pits was that the plate-like pits were sharp in Cicada I and wide in Cicada II. This may due to the differences in the internal defects of the crystals. However, it is difficult to determine the internal crystal defects that exist under the etch pits merely by observing them from the surface using SEM or AFM.

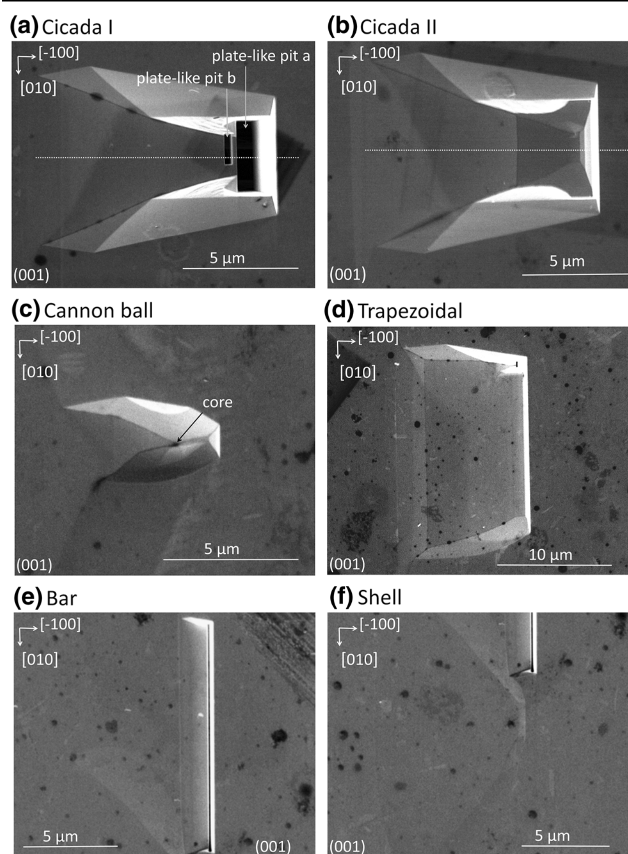

Fig. 1. SEM images of six differently shaped etch pits on β-Ga_2O_3 (001). (a) Cicada I-type. (b) Cicada II-type. (c) Cannon ball-type. (d) Trapezoidal-type. (e) Bar-type. (f) Shell-type.

MATERIALS AND METHOD

In this study, to understand the differences in internal defects under the etch pits, we observed them three-dimensionally by repeating cross-sectional processing using a focused ion beam (FIB) and SEM image capture with an electron beam (EB). This method is the so-called FIB tomography, Slice & View, or Cut & See.[12] There are no previous reports of this method being applied to crystal defect analysis in β-Ga_2O_3. Figure 3 shows a schematic of this observation method. We used a Thermo Fisher Scientific Helios FIB–SEM for this study, which was able to perform both FIB processing and continuous SEM image observation with an EB. The etch pits investigated in this study were Cicada I and Cicada II, which had the same characteristic shapes that were observed in previous SEM and AFM analysis (Figs. 1a, b and 2).[11] Etching was performed using a KOH + NaOH solution at 200°C for 2 min.[13] Several 100 nm of carbon were deposited on the etch pits to protect the surface prior to the FIB cross-section processing, which, together with SEM image capturing, was repeated at 100-nm intervals in the [0–10] direction (Fig. 3). SEM observation was performed at 2 kV/0.1 nA, and secondary electron images were acquired. The FIB for cross-sectional processing was inclined at an angle of 52° with respect to the EB. Therefore, the cross-sectional SEM images in this report are oblique images that have been captured with the samples tilted at an angle of 52°.

RESULTS AND DISCUSSION

Figure 4a–y show a series of cross-sectional SEM images of the Cicada I-type etch pit, observed using the procedure described above (Fig. 3) and shown at 200-nm intervals. During AFM measurement in Fig. 2a, the depth of plate-like pit a was estimated to be approximately 4 μm. However, this method revealed that the actual depth was approximately 10 μm, as shown in Fig. 4p. Furthermore, close to the surface, the thickness of plate-like pit a was approximately 1.2 μm and decreased to approximately 400 nm as the depth increased, as shown in Fig. 4j and q. Plate-like pit b was also clearly captured, as shown in Fig. 4n and o. Both these plate-like pits were sharp voids and were inclined at an angle of approximately 76° against the (001) plane. In other words, they occurred along the [001] direction or the (100) plane. In addition, the widths of plate-like pits a and b were observed at approximately 3 and 1 μm in the [010] direction, respectively. Moreover, a change in contrast can be observed under plate-like pit b, as shown in the high-brightness regions in Fig. 4i–q. This change in contrast was also along the [001] direction and had a width of approximately 2 μm in the [010] direction, as shown in Fig. 4l–q. Figure 5a–y show a series of cross-sectional SEM images of the Cicada II-type etch pit. These SEM images are shown at

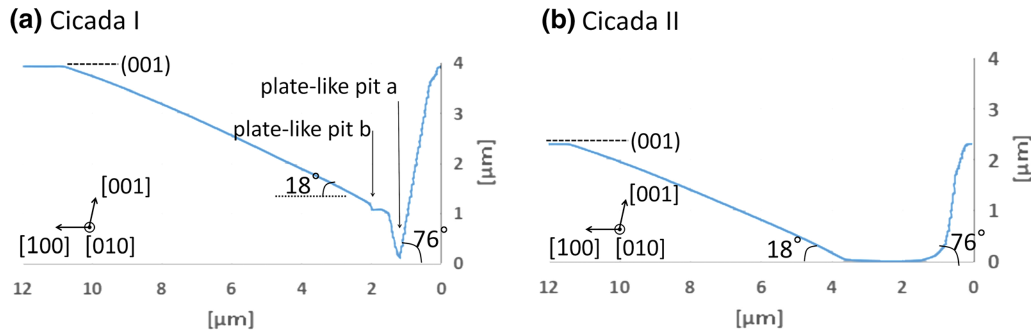

Fig. 2. (a) and (b) Depth profiles along the dotted line in Fig. 1a and b, respectively.

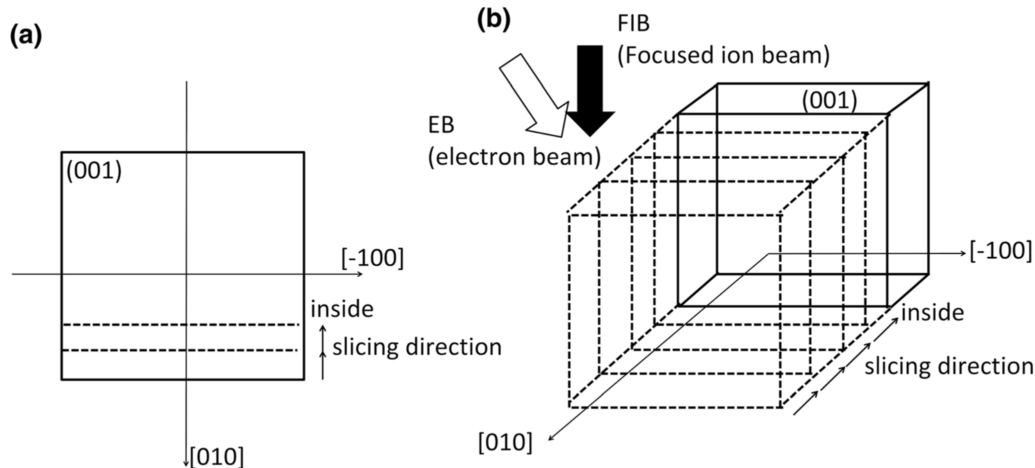

Fig. 3. Schematics of the three-dimensional SEM observation. (a) Top view. (b) Three-dimensional view.

200-nm intervals in the [0–10] direction. The depth of the plate-like pit of Cicada II was approximately 2 μm, which agreed with the AFM measurement result. In addition, the sharp voids observed in the plate-like pits a and b of Cicada I were not observed, and the shape having a width in the [100] direction was the same as the result of AFM analysis. The contrast change in the SEM image observed under the plate-like pit b of Cicada I was also observed in Cicada II, as shown in the high-brightness regions in Fig. 5n–x. Figure 6 shows an enlargement of a part of the cross-sectional SEM image where the high-brightness regions were observed. The high-brightness region observed in Cicada II was also along the [001] direction, and its width was approximately 2 μm in the [010] direction.

These results show that this method revealed not only the accurate shape measurement of the plate-like pit, but also the existence of the area under the plate-like pit, which was observed as a high-brightness region in the SEM image. This could not be clarified using surface SEM observation or AFM measurement. Therefore, the three-dimensional observation of the etch pits using FIB–SEM is an effective method for understanding the internal state of the crystals. In addition, this contrast change in the SEM images observed under the plate-like pits (shown in the high-brightness regions in Figs. 4 and 5) can be considered to be the difference in secondary electron emission coefficient due to the difference in crystal structure. Furthermore, this region not only extends in the [001] direction but also has a width of approximately 2 μm in the [010] direction. That is, it has a planar shape along the (100) plane. From these results, we conclude that this high-brightness regions under the plate-like pits are due to planar defects. Incidentally, Yamaguchi et al.[9] reported the slip planes of β-Ga_2O_3 as {−201}, {101}, {−301}, and {−3−10}, and Ueda et al.[6] reported the existence of twin lamella along the (100) plane. Therefore, we speculate that the planar defects under the plate-like pits are SFs caused by a combination of slip planes such as the {−201} and {101}, or SFs caused by twin lamella. From the above discussion, we consider that Cicada I is an etch pit shape in which the plate-

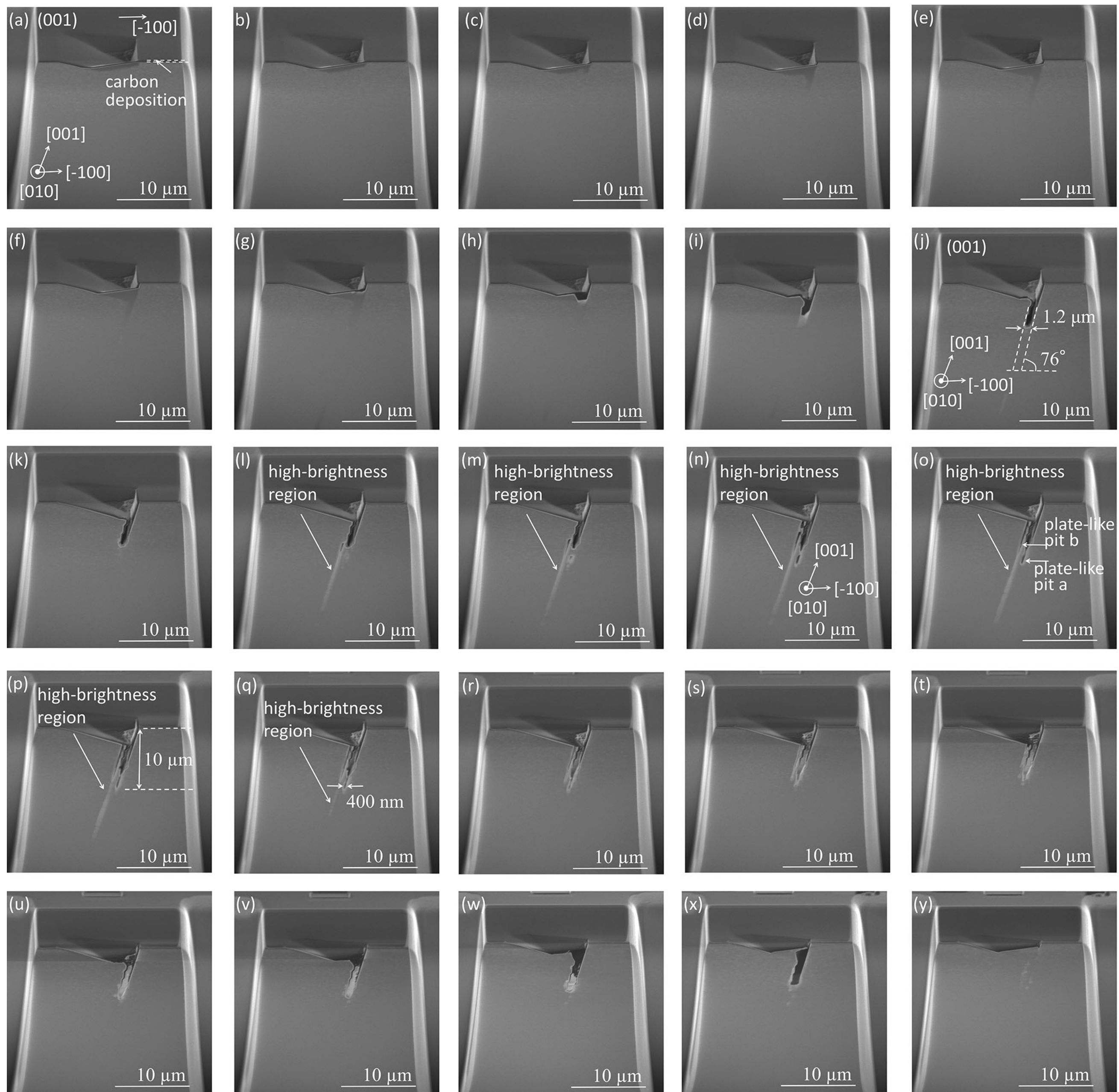

Fig. 4. Cross-sectional SEM images of the Cicada I-type etch pit of β-Ga_2O_3 (001). These SEM images were acquired with the sample tilted at 52°. SEM images (a)–(y) were captured with an interval of 200 nm toward the [0–10] direction. The numbers displayed in the figure are the values corrected for the effect of oblique SEM observation at 52°.

like void and “SFs” are mixed, and Cicada II is an etch pit mainly caused by SFs. To confirm this, high-resolution TEM observation is required.

CONCLUSION

FIB–SEM was used for the three-dimensional observation of etch pits to directly capture the internal defects of a crystal. Using this technique on the etch pits of Cicada I and Cicada II that were observed on a β-Ga_2O_3 (001) wafer after etching, we found a plate-like void and contrast change in the SEM image inside the crystal. Moreover, we found that these had a planar shape along the (100) plane. From these results, we conclude that the proposed method is an effective way for understanding the internal defects of a crystal that cannot be revealed by observing the surface using SEM and AFM analysis. In addition, we conclude that the change in the SEM image contrast is due to planar defects, and we infer that Cicada I is an etch pit shape in

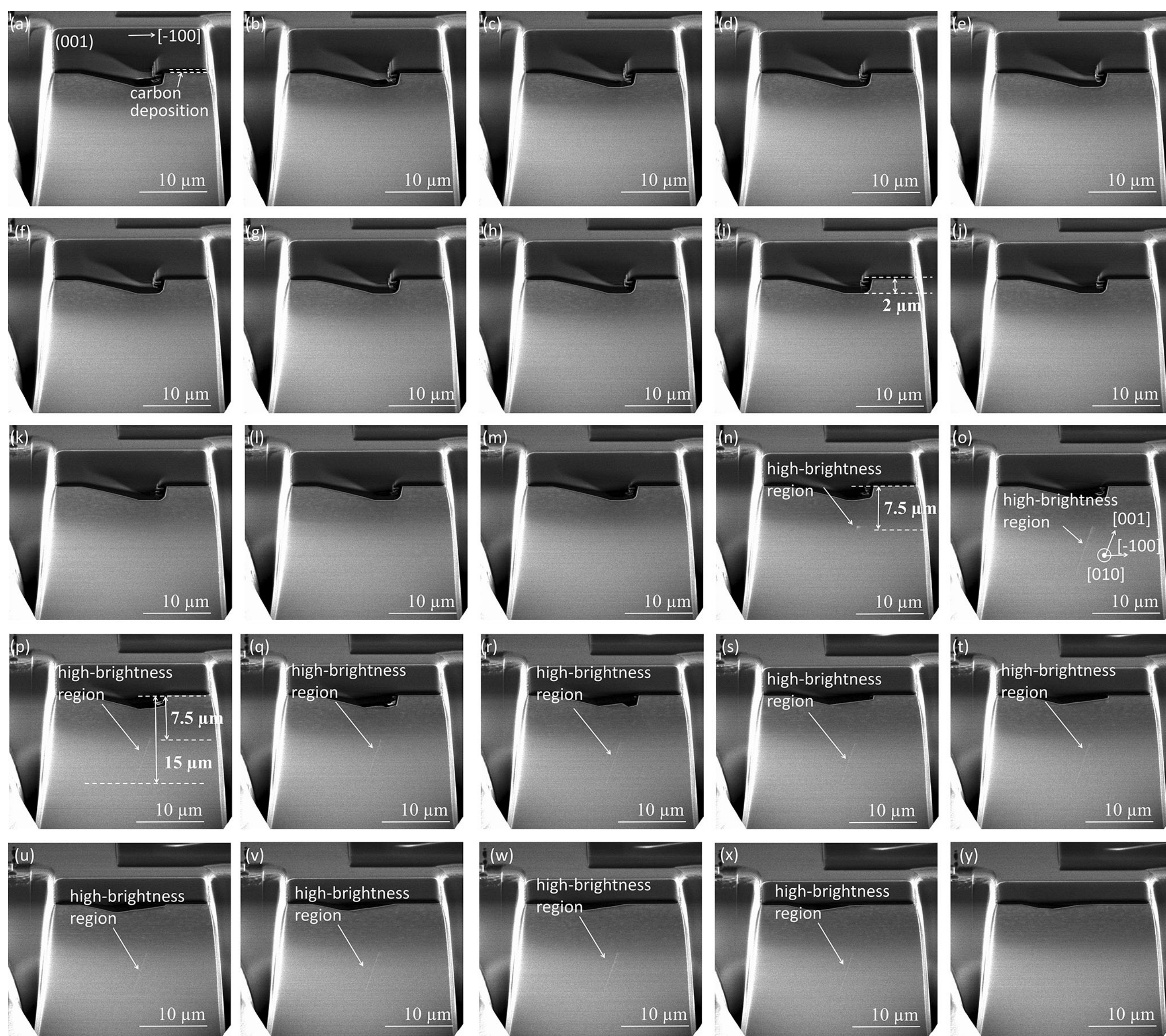

Fig. 5. Cross-sectional SEM images of the Cicada II-type etch pit of β-Ga_2O_3 (001). These SEM images were acquired with the sample tilted at 52°. SEM images (a)–(y) were captured with an interval of 200 nm toward the [0–10] direction. The numbers displayed in the figure are the values corrected for the effect of oblique SEM observation at 52°.

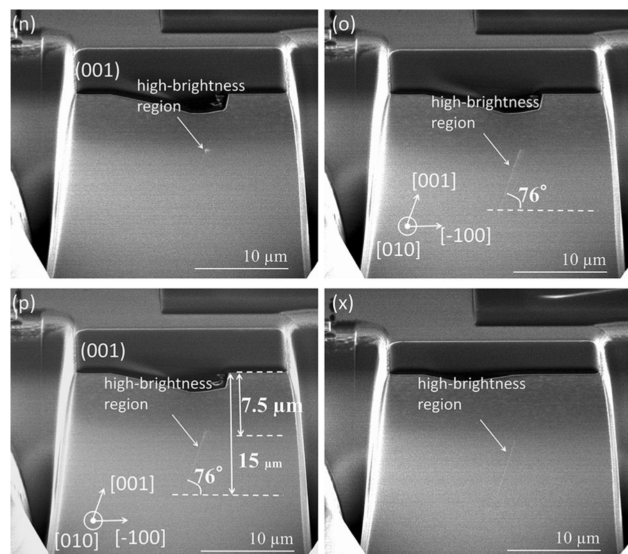

Fig. 6. Enlarged images of Fig. 5n, o, p, and x.

which the plate-like void and SFs are mixed and that Cicada II is an etch pit caused by SFs.

CONFLICT OF INTEREST

The authors declare no conflict of interest associated with this manuscript.

REFERENCES

1. S. Geller, *J. Chem. Phys.* 33, 676 (1960).
2. S.J. Pearton, J. Yang, P.H. Cary, F. Ren, J. Kim, M.J. Tadjer, and M.A. Mastro, *Appl. Phys. Rev.* 5, 011301 (2018).
3. H. Aida, H. Nishiguchi, H. Takeda, N. Aota, K. Sunakawa, and Y. Yaguchi, *Jpn. J. Appl. Phys.* 47, 8506 (2008).
4. A. Kuramata, K. Koshi, S. Watanabe, Y. Yamaoka, T. Masui, and S. Yamakoshi, *Jpn. J. Appl. Phys.* 55, 1202A2 (2016).
5. K. Nakai, T. Nagai, K. Noami, and T. Futagi, *Jpn. J. Appl. Phys.* 54, 051103 (2015).
6. O. Ueda, N. Ikenaga, K. Koshi, K. Iizuka, A. Kuramata, K. Hanada, T. Moribayashi, S. Yamakoshi, and M. Kasu, *Jpn. J. Appl. Phys.* 55, 1202BD (2016).
7. K. Hanada, T. Moribayashi, K. Koshi, K. Sasaki, A. Kuramata, O. Ueda, and M. Kasu, *Jpn. J. Appl. Phys.* 55, 1202BG (2016).
8. M. Kasu, T. Oshima, K. Hanada, T. Moribayashi, A. Hashiguchi, T. Oishi, K. Koshi, K. Sasaki, A. Kuramata, and O. Ueda, *Jpn. J. Appl. Phys.* 56, 091101 (2017).
9. H. Yamaguchi, A. Kuramata, and T. Masui, *Superlatice Microstruct.* 99, 99 (2016).
10. H. Yamaguchi and A. Kuramata, *J. Appl. Cryst.* 51, 1372 (2018).
11. K. Ogawa, N. Ogawa, R. Kosaka, T. Isshiki, Y. Yao and Y. Ishikawa, *Abs. ICSCRM2019*, Kyoto, Japan (2019).
12. L. Holzer, F. Indutnyi, P.H. Gasser, B. Münchi, and M. Wegmann, *J. Microscopy* 216, 84 (2004).
13. Y. Yao, Y. Ishikawa, and Y. Sugawara, *Phys. Status Solidi. A* 217, 1900630 (2019).

Publisher's Note Springer Nature remains neutral with regard to jurisdictional claims in published maps and institutional affiliations.